



**HAL**  
open science

# Ultimate electromechanical energy conversion performance and energy storage capacity of ferroelectric materials under high excitation levels

Nguyen Thanh Tung, Gaspard Taxil, Hung Hoang Nguyen, Benjamin Ducharne, Mickaël Null Lallart, Elie Lefeuvre, Hiroki Kuwano, Gaël Sebald

## ► To cite this version:

Nguyen Thanh Tung, Gaspard Taxil, Hung Hoang Nguyen, Benjamin Ducharne, Mickaël Null Lallart, et al.. Ultimate electromechanical energy conversion performance and energy storage capacity of ferroelectric materials under high excitation levels. *Applied Energy*, 2022, 326, pp.119984. 10.1016/j.apenergy.2022.119984 . hal-03836257

**HAL Id: hal-03836257**

**<https://hal.science/hal-03836257>**

Submitted on 2 Nov 2022

**HAL** is a multi-disciplinary open access archive for the deposit and dissemination of scientific research documents, whether they are published or not. The documents may come from teaching and research institutions in France or abroad, or from public or private research centers.

L'archive ouverte pluridisciplinaire **HAL**, est destinée au dépôt et à la diffusion de documents scientifiques de niveau recherche, publiés ou non, émanant des établissements d'enseignement et de recherche français ou étrangers, des laboratoires publics ou privés.

# Ultimate electromechanical energy conversion performance and energy storage capacity of ferroelectric materials under high excitation levels

Nguyen Thanh Tung<sup>1</sup>, Gaspard Taxil<sup>1,2</sup>, Hung Hoang Nguyen<sup>3,4</sup>, Benjamin Ducharme<sup>1</sup>, Mickaël Lallart<sup>2</sup>, Elie Lefeuvre<sup>5</sup>, Hiroki Kuwano<sup>1,3,4</sup>, Gael Sebald<sup>1</sup>

<sup>1</sup>*ELyTMaX IRL3757, CNRS, Univ Lyon, INSA Lyon, Centrale Lyon, Universite Claude Bernard Lyon 1, Tohoku University, Sendai, Japan*

<sup>2</sup>*Univ. Lyon, INSA-Lyon, LGEF EA682, F-69621, France*

<sup>3</sup>*New Industry Creation Hatchery Center (NICHe), Tohoku University, 6-6-10 Aramaki-Aoba, Aoba-ku Sendai, Miyagi 980-8579, Japan*

<sup>4</sup>*Sendai Smart Machines Co., Ltd. (SSM), 6-6-40 Aza-Aoba, Aramaki, Aoba-ku, Sendai, Miyagi 980-8579, Japan*

<sup>5</sup>*Centre for Nanoscience and Nanotechnology, University of Paris-Saclay - CNRS, Palaiseau, France*

**Abstract:** In the framework of piezoelectric energy harvesting, this work focused on the quantification of the ultimate energy conversion capability of various ferroelectric ceramics and single crystals. Energy conversion was achieved by the application of Ericsson cycles under high electric field and mechanical stress. The main aim of this approach was to experimentally apply the electromechanical Ericsson cycles on several key materials. This process was decomposed into four steps, which consisted of applying and removing an electric field under constant stress and stress application/removal under a constant electric field. In this work, ferroelectric ceramics—hard PZT C203, medium PZT C6, soft PZT C9, and single crystal PMN-25PT and PZN-8PT— and paraelectric ceramic PMN 15 were tested. The PMN-25PT and PZN-8PT ferroelectric single crystals exhibited higher energy conversion potential than the ceramics in the ferroelectric and paraelectric phases. However, the soft PZT C9 ceramic (107.6 mJ/cm<sup>3</sup>) was comparable to single crystal PMN-25PT (118.7 mJ/cm<sup>3</sup>). Considering the cost and fabrication process, PZT C9 is an excellent candidate for practical applications. A simple yet accurate experimental estimation of the energy density of the materials based on the bipolar hysteresis curves under compressive stresses of 1 and 100 MPa was also proposed. The estimated energy densities were similar to the real Ericsson cycles. The energy storage capacity of these materials was also analyzed. The PMN 15 ceramic in the paraelectric phase had the highest stored energy, and in the paraelectric phase, PMN 15 had a maximum stored electrical energy of 87 mJ/cm<sup>3</sup> under a static stress value of 1 MPa, which was increased to 105 mJ/cm<sup>3</sup> under a static stress value of 100 MPa. Ultimately, this study allowed for the evaluation of the maximal energy conversion capabilities of several classes of electroactive materials, highlighting their potential in terms of their target applications and operative environments (such as the maximal stress or electric field).

**Keywords:** Ericsson cycle, energy density, energy storage, compressive stress, energy harvesting, ferroelectric

## 1. Introduction

Ferroelectric materials are considered potential materials for numerous energy harvesting [1,2] and energy / information storage [3–5] applications, such as vibrational microgenerators and non-volatile random-access memory. These types of materials are typically pyroelectric and piezoelectric when operating below their Curie temperature. Ferroelectric materials exhibit spontaneous polarization, which can be reoriented or reversed by applying an appropriate and significant electric field in the opposite direction. Based on this property, information could be stored as ferroelectric polarization for non-volatile memory applications [6,7]. In addition to the paraelectric phase (cubic phase), numerous potential ferroelectric phases exist depending on the shape and polarization of the unit cell, with rhombohedral, orthorhombic, and tetragonal phases being the most common. When a ferroelectric material is in the paraelectric phase above its Curie temperature, it loses its piezoelectric properties.

Energy harvesting consists of converting ambient energy sources into electrical energy, accumulating and storing it for later use [8]. This process has emerged as a promising technique for supplying sensors and sensor networks, limiting the use of natural resources while providing a reliable long-term energy source, especially compared to batteries, which suffer from self-discharge issues. With improvements in nano/microelectronics technology, electronic devices continue to decrease in size, resulting in continuous reduction in power consumption for given operations. Thus, harvested energy may be sufficient to partially or entirely replace batteries in the frameworks of wireless sensors and sensor networks that operate discontinuously. Recently, flexible piezoelectric nanogenerators have shown great potential for the next generation of wearable electronic-based devices for human health and movement monitoring [9,10]. Energy harvesting can generate electricity from several sources, including kinetic, thermal, solar, or electromagnetic energy [11–15]. Human activities such as walking or opening a door are also considered an attractive energy source for mechanical energy harvesting using dielectric or electromagnetic transduction methods [16,17]. For piezoelectric energy harvesting, most of the proposed devices work as resonators harvesting energy from vibrations. The energy density per cycle can range from  $10 \mu\text{J}/\text{cm}^3$  to  $25 \text{mJ}/\text{cm}^3$  [18] of the active material at most. However, such a value is solely based on empirical analysis of achieved experimental devices. Until now, no investigation has been conducted on the theoretical limit in terms of convertible and harvestable energy, although such a study would: 1) allow a comparison of the performance of energy harvesters with respect to the ultimate energy that can actually be harvested (i.e., in a similar way to the Carnot efficiency for thermal devices) and 2) provide insights into the design of optimized harvesters to work close to their theoretical limits in terms of output energy. In contrast, research efforts have been made to investigate the pyroelectric energy conversion capabilities of ferroelectric materials through Olsen or Ericsson cycles, with output energies far above those given by the linear pyroelectric coefficient

[19–25]. However, the maximum amount of energy that can be harvested through electromechanical coupling using ferroelectric materials is still unknown; however, it is of primary importance [26].

Ericsson cycles include two iso-fields and two iso-stresses loadings, which were used in this study to estimate the energy conversion performance of ferroelectric materials. Previous studies have demonstrated that coupling an electric field and mechanical excitation through Ericsson cycles yielded a significant increase in harvested energy [27,28]. This study investigated the energy conversion performance of various ferroelectric ceramics and single crystals that underwent ferroelectric and paraelectric phases through Ericsson cycles. We also developed a simple and accurate semi-empirical estimation of energy density based on bipolar hysteresis curves (P-E loops) under compressive stresses of 1 and 100 MPa. The ferroelectric phase of lead zirconate titanate (PZT) ceramics (hard PZT C203, medium PZT C6, soft PZT C9), single crystal lead magnesium niobate-lead titanate (PMN-25PT), single crystal lead zinc niobate-lead titanate (PZN-8PT), and the paraelectric phase of ceramic PMN 15 were characterized. The objective of this study was to estimate the ultimate energy conversion capability of ferroelectric materials under intermediate and high levels of stresses and electric fields. Finally, as a complementary investigation, these materials were also assessed for electrical energy storage applications.

## **2. Experimental methods**

### ***2.1. Materials and testbench***

Disk-shaped electrostrictive PMN 15 ceramics (10 mm in diameter and 1 mm thick, with silver electrodes) were purchased from TRS Technologies, State College, PA, USA. PMN 15 exhibited a maximal dielectric constant at 15°C and was in the paraelectric phase at room temperature. Hard, medium, and soft piezoelectric lead zirconate titanate ( $\text{Pb}(\text{ZnTi})\text{O}_3$ ) (PZT) ceramics C203, C6, and C9 were purchased from Fuji Ceramics Corporation, Fujinomiya, Japan. In addition, single crystal [001]-oriented lead-magnesium niobate-lead titanate PMN-25PT was purchased from Otsuka Corporation, Japan, and [001]-poled single crystal lead zinc niobate-lead titanate PZN-8PT was purchased from Microfine Materials Technologies, Singapore. All samples had the same thickness of 1 mm. [Table 1](#) shows the properties of these samples. PZT C203, C6, C9, and PMN-25PT with a section of 6 x 6 mm<sup>2</sup> and PZN-8PT (2.5 x 2.5 mm<sup>2</sup>) were cut by a dicing machine (DISCO, DAD3240). Photographs of the samples are shown in [Figure 1c](#). Then, the cut samples were poled in a silicone oil bath using the field cooling technique [29]. The treated samples were heated to the desired temperature (200, 180, 130, 90, and 150°C for PZT C203, C6, C9, PMN-25PT, and PZN-8PT, respectively), where an electric field of 3 kV/mm was applied for 30 min and maintained while cooling down. When the sample temperature reached room temperature, the electric field was powered off, and the sample was removed. The Ericsson cycles and bipolar cycle measurements could also act as a poling process, which would be sufficient for most of the tested materials. However, for hard PZT, it was necessary to pole it

beforehand, as the material could not be poled at room temperature. For the other materials, if the electric field was not very high compared to the coercive field, we could have partially maintained a depolarized state during the cycle, which would be detrimental to the piezoelectric activity. As a result, we chose to prepare the fully poled samples as a reference status before applying the electric field and mechanical stress

Figure 1a shows a schematic diagram of the measurement system, where a Tektronix® AFG1022 arbitrary function generator and Trek® 10/10B-HS high voltage amplifier were used to apply the electric field. A Shimadzu® AGS-X series traction machine was used to apply compressive stress to the sample, as shown in Figure 1b. The current through the sample was monitored using a low-noise current amplifier (Stanford research®, Sunnyvale, CA, United States of America), and a Digilent® data acquisition system (Pullman, WA United States of America) was used to monitor and record the applied voltage and electrical current. An overload protection circuit was used to protect the measuring system, and the sample under test was immersed in silicone oil to avoid electric arcing during measurement.

Materials	C203	C6	C9	PMN-25PT [30][31]	PZN-8PT	PMN 15 [32][33]
Coupling factor $k_{33} \times 10^{-2}$	71	76	69	91–94.9	94	60
Dielectric constant $\epsilon_{33}^T/\epsilon_0$	1450	2130	6640	5400–5493	7700	~ 24000
Piezoelectric coefficient $d_{33} \times 10^{-12}(\text{C/N})$	325	427	718	1540–2060	2890	700 Peak value

Table 1: Properties of PZT C203, C6, C9, PMN-25PT, PZN-8PT, and PMN 15, as obtained from the suppliers

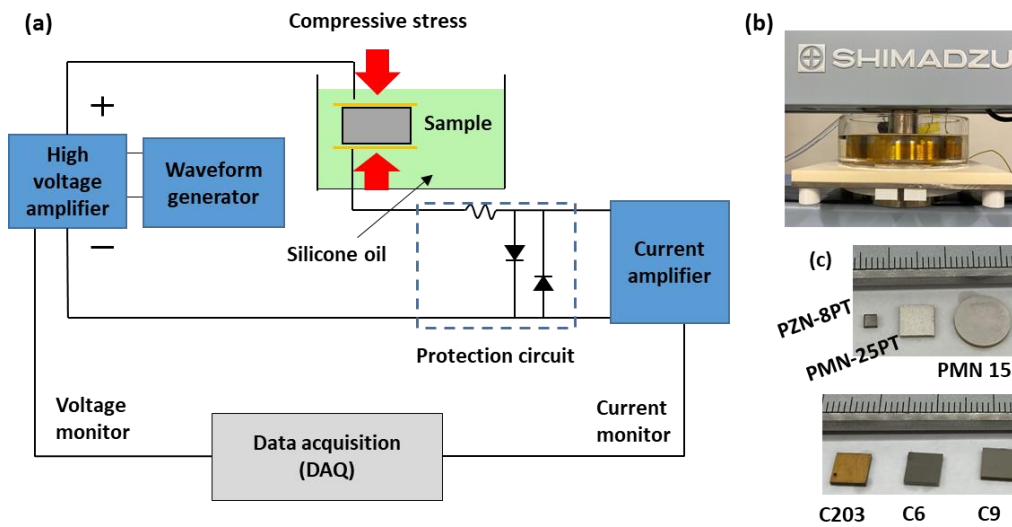


Figure 1: (a) Schematic diagram of the measurement system to obtain the Ericsson cycles and bipolar P-E loops, (b) photograph of the sample under compressive stress using a Shimadzu electromechanical test frame, and (c) photographs of the tested samples.

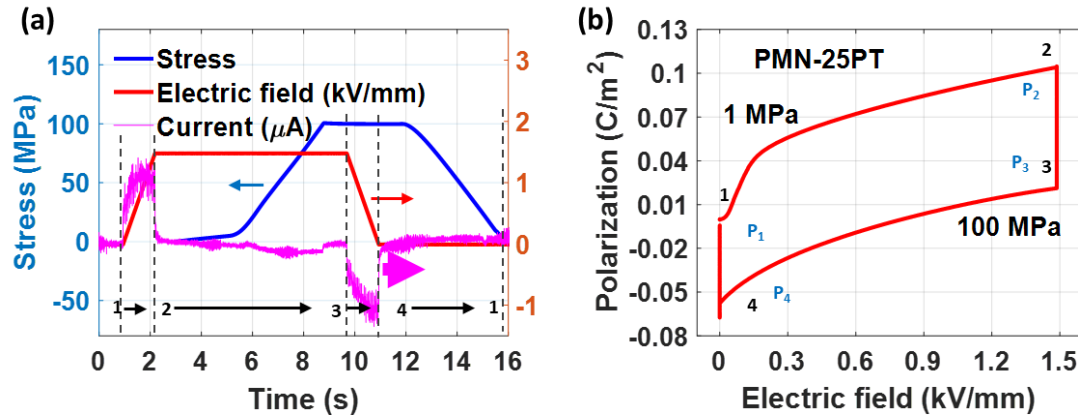


Figure 2: (a) Waveforms of the applied electric field and compressive stress for the Ericsson cycles (1 MPa and 100 MPa, which were applied on PMN-25PT for illustration); (b) Ericsson cycle of PMN-25PT for illustration. In processes 1–2, the electric field was increased from 0 to 1.5 kV/mm under constant compressive stress of 1 MPa. In processes 2–3, the compressive stress was increased from 1 to 100 MPa under a constant 1.5 kV/mm electric field. In processes 3–4, the electric field was decreased from 1.5 to 0 kV/mm under a constant 100 MPa compressive stress. In processes 4–1, compressive stress was released from 100 MPa to 1 MPa under a constant 0 kV/mm electric field.

## 2.2. Ericsson cycle application and analysis methods

Ericsson cycles are used to convert thermal or mechanical energy into electrical energy with ferroelectric materials [22–25]. Figure 2a shows the electric field and compressive stress waveforms during the Ericsson cycle, where compressive stresses of 1 and 100 MPa were applied to the PMN-25PT sample. A low-stress value of 1 MPa was chosen to ensure good electrical contact, and the applied electric field was swept from 0 to 1.5 kV/mm for all samples. Polarization was calculated by integrating the current in time. Figure 2b shows a PMN-25PT Ericsson cycle as a representative example. Between steps 1 and 2, the electric field increased from 0 to a high electric field (1.5 kV/mm) for 1 second under a constant low compressive stress level of 1 MPa.

The polarization was increased following the electric field variations. Electrical energy was transferred from the voltage amplifier to the sample, whose polarization changed from  $P_1$  to  $P_2$  (equivalent to capacitor charging). From steps 2 to 3, the compressive stress increased from 1 to 100 MPa for 6 s under a constant electric field of 1.5 kV/mm. The applied compressive stress induced the reduction of polarization from  $P_2$  to  $P_3$ , which could be used to harvest electrical energy [34–37]. This polarization drop originated from the switching phenomenon of the ferroelectric domains during mechanical depolarization and the phase transitions induced by mechanical stress. From step 3 to step 4, the applied electric field decreased from 1.5 kV/mm to 0 for 1 second under constant compressive stress of 100 MPa. The polarization decreased following the reorientation of the ferroelectric domains, resulting in a small amount of discharging current. From steps 4 to 1, the compressive stress was released to the original value of 1 MPa to complete the Ericsson cycle. All Ericsson cycles were performed at room temperature (20°C). The area of the Ericsson cycle (1-2-3-4) was equivalent to the

converted mechanical energy density of the sample under test. Similar to the Olsen cycle [38,39], this area could be calculated by Eq. 1 [22–25]:

$$W = \oint \frac{E \cdot dP}{A} = \oint \frac{P \cdot dE}{A}, \quad (\text{Eq. 1})$$

where P, E, and A denote the polarization, electric field, and sample area, respectively. All tests consisted of three consecutive cycles to avoid polarization irreversibility issues, and only data from the last cycle was monitored.

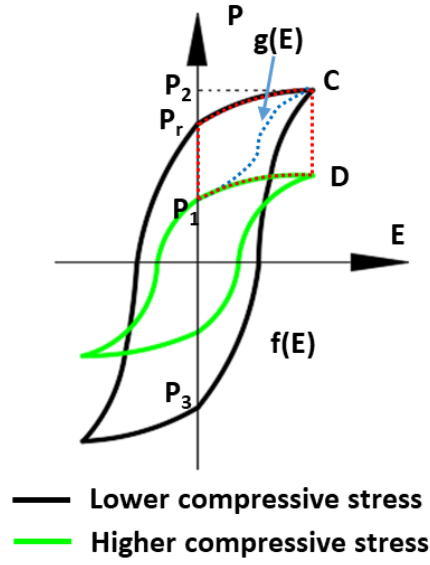


Figure 3: Bipolar P-E loops under lower and higher compressive stresses, with the estimated Ericsson cycle P1-Pr-C-D-P1 using descending-descending curves of bipolar P-E loops (Estimation 1). Our semi-empirical estimated Ericsson cycle P1-g(E)-C-D-P1 was based on the first-order reversal curves.

### 2.3. Bipolar P-E loops-based estimated Ericsson cycles

In Uruan et al. and Patel et al. [22,23], the Ericsson cycle energy densities were estimated using the two descending curves of the bipolar P-E loops under low and high stresses, respectively (P1-Pr-C-D-P1 cycle in Figure 3). However, this technique was imprecise due to the irreversibility of the polarization decrease under such high stress (hysteresis issue). In this work, an alternative semi-empirical estimation technique was considered, in which the ascending curve of the P-E loop under low-stress  $f(E)$  shifted upward to become  $g(E)$ , which was equivalent to a first-order reversal curve [40]. Hence, the estimated Ericsson cycle became the P1-g(E)-C-D-P1 cycle, where  $g(E)$  was calculated from  $f(E)$  according to the following relation:

$$g(E) = f(E) \cdot \frac{P_2 - P_1}{P_2 - P_3} + P_1 - P_3 \cdot \frac{P_2 - P_1}{P_2 - P_3}, \quad (\text{Eq. 2})$$

The bipolar P-E loops of all samples were obtained by applying a sinusoidal voltage of 1 Hz and an electric field of  $\pm 1.5$  kV/mm.

## 2.4. Energy storage

In addition to the energy conversion assessment, the potential applications of these ferroelectric and paraelectric materials as electrostatic capacitors were considered. The energy storage capacity could be estimated by the surface integral of the bipolar P-E loops [24,41,42]:

$$U = \oint_{P_r}^{P_{max}} \frac{E \cdot dP}{A}, \quad (\text{Eq. 3})$$

where  $P_r$  and  $P_{max}$  denote the remnant and maximum polarization values, respectively.

## 3. Results

Energy conversion performance was first investigated (from 1 to 100 MPa compressive stress, electric fields of 0 to 1.5 kV/mm) using Ericsson cycles for PZT C203, C6, C9, PMN-25PT, PZN-8PT, and PMN 15 under significant compressive stress variations (Figure 4). This was followed by intermediate compressive stress variations (from 1 to 30 MPa compressive stress, electric fields of 0 and 1.5 kV/mm) (Figure 5). Comparisons of the converted energy densities for the high and intermediate mechanical variations are shown in Figures 6a and 6b. For the high variations (Figure 6a), and considering the ferroelectric phase ceramics, the energy density was smaller for hard PZT C203, larger for medium PZT C6, and much larger for soft PZT C9. The ferroelectric phase single crystals (PMN-25PT, PZN-8PT) exhibited excellent energy density, especially PZN-8PT, which had tremendous values. Regarding the paraelectric phase material, the energy density of PMN 15 was smaller than the ferroelectric phase materials. The application of mechanical compressive stresses under a constant electric field of 1.5kV/mm induced polarization decreases as low as  $\Delta P = P_2 - P_3$  of 49.7, 66.0, 70.2, 83.5, 208, and 36.6 mC/m<sup>2</sup> for ferroelectric phase ceramics of hard PZT C203, medium PZT C6, soft PZT C9, single crystal PMN-25PT and PZN-8PT, and paraelectric phase PMN 15, respectively. This polarization decrease was the smallest for the paraelectric phase PMN 15, smaller for hard PZT C203, larger for medium PZT C6, much larger for soft PZT C9, and the greatest for the PMN-25PT, PZN-8PT single crystal. The reduction in polarization at an electric field of 1.5 kV/mm, by increasing the compressive stress from 1 to 100 MPa, could be roughly estimated by an equivalent effective piezoelectric coefficient  $d_{33\_eff}$  (at 1.5 kV/mm):

$$\Delta P = d_{33\_eff} \cdot \Delta T_3, \quad (\text{Eq. 4})$$

where  $\Delta T_3$  is the applied stress difference in the 3-direction (z-direction). This value was smaller for hard PZT, larger for soft PZT, and the largest for the single crystal ferroelectric materials, resulting in different influences of compressive stresses on polarization reduction. The ferroelectric materials in the paraelectric phase lost their piezoelectric properties; thus, the energy density of the PMN 15 was the smallest. The same tendency was observed at the intermediate level (Figure 6b). The energy

densities of PMN-25PT and PZN-8PT single crystals were much higher than the other materials. For high-level variations, the energy density of the PZT ceramic C9 was comparable to the PMN-25PT single crystal. In the framework of a realistic energy harvester, considering the cost and complexity of fabrication process, PZT C9 (or similar soft PZT materials) appeared to be a plausible candidate for future applications.

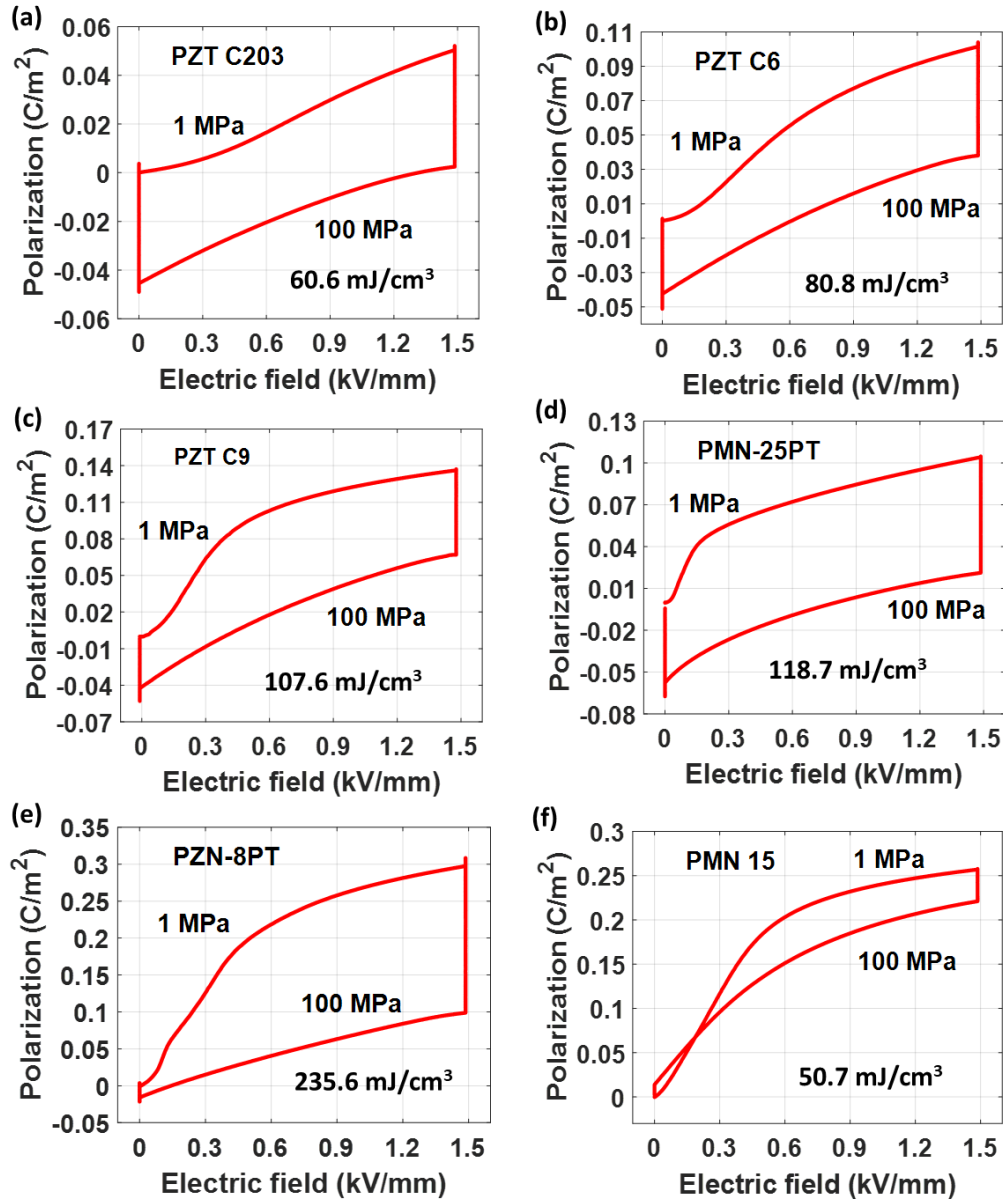


Figure 4: The Ericsson cycles of PZT C203, C6, C9, PMN-25PT, PZN-8PT, and PMN 15 at high levels of compressive stress of 1 and 100 MPa, with 0 and 1.5 kV/mm electric fields.

To finalize the analysis, much lower stresses and electric field levels were also considered. When limiting the electric field to 100 V/mm and the mechanical stress to 1 MPa, we could assume that the material would remain in its linear region, both in terms of the electric and mechanical responses.

In this case, the Ericsson cycle energy density was simplified as:

$$W = d_{33} \cdot T \cdot E, \quad (\text{Eq. 5})$$

where  $d_{33}$  (C/N) denotes the piezoelectric coefficient,  $T$  (Pa) the stress, and  $E$  (V/m) the electric field.

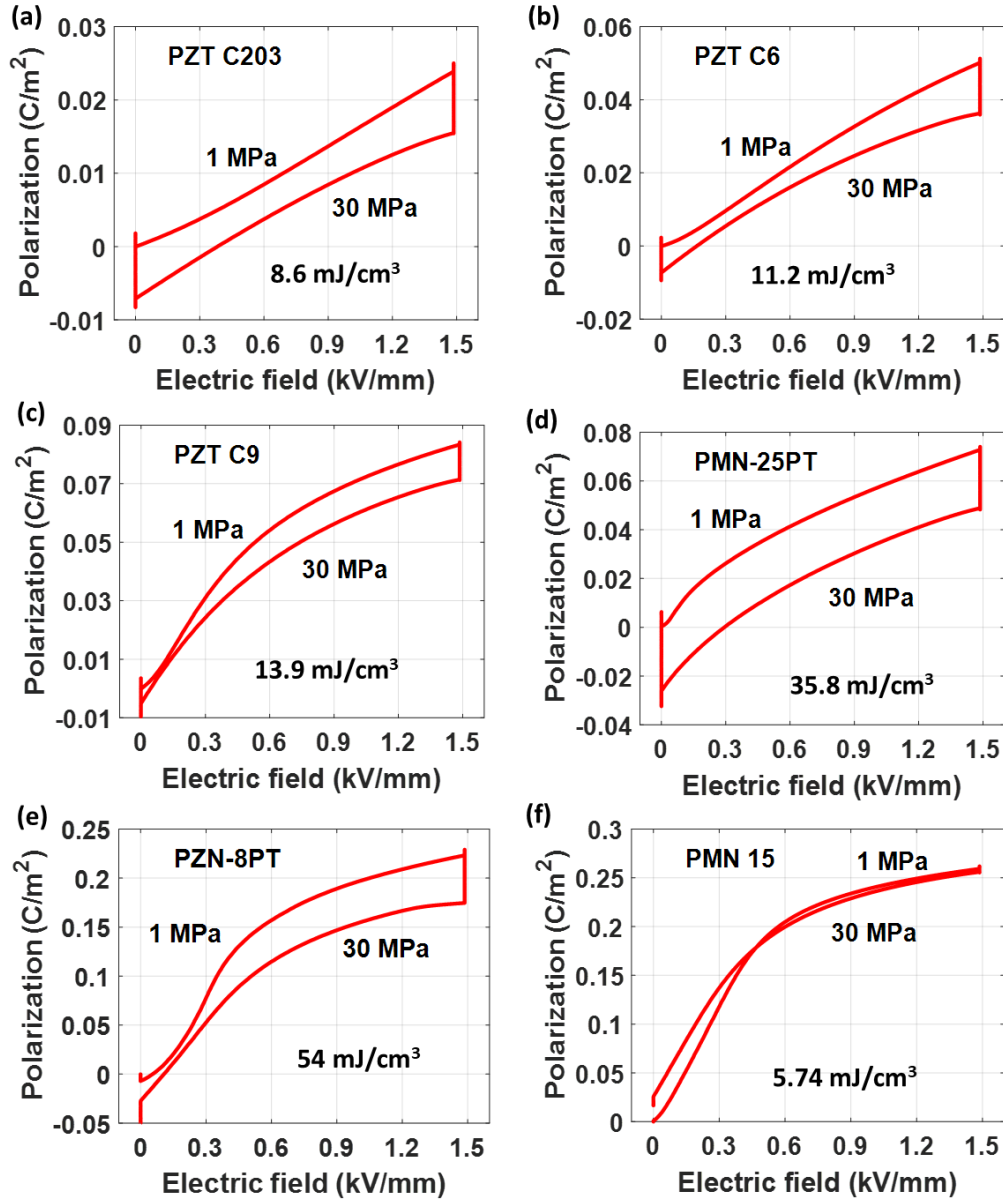


Figure 5: The Ericsson cycles of PZT C203, C6, C9, PMN-25PT, PZN-8PT, and PMN 15 at intermediate level of compressive stress of 1 and 30 MPa, and 0 and 1.5 kV/mm electric fields.

The piezoelectric coefficients of PZT C203, C6, C9, PMN-25PT, PZN-8PT, and PMN 15 are shown in Table 1. The piezoelectric coefficient of PMN 15 was deduced to be around 50 (pC/N), and the energy densities in this case are given in Figure 6c. The energy densities of these samples at low levels manifested the same tendency as those observed at high and intermediate levels.

Predicting these values from the bipolar P-E loops may also be of significant interest, to quickly assess the energy conversion and harvesting performance. Hence, an Ericsson cycle energy density estimation was conducted for PZT C6 from the descending curves [22,23] and compared to the experimental Ericsson cycles.

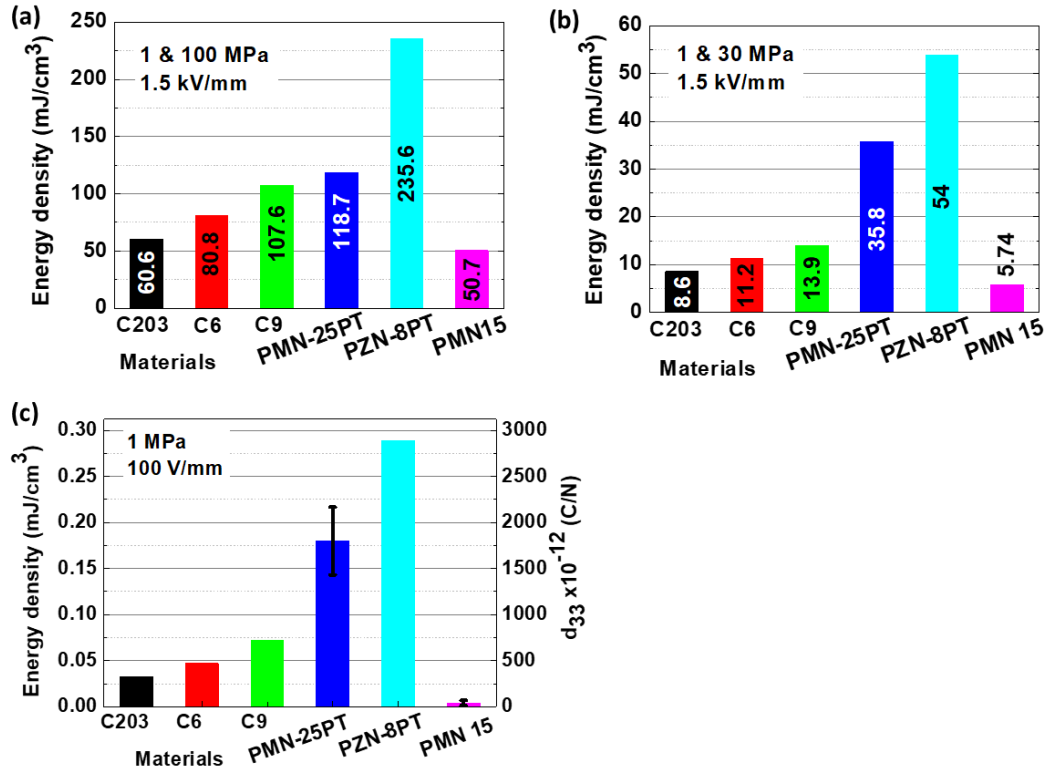


Figure 6: Energy densities of samples (a) at high (1 and 100 MPa, 0 and 1.5 kV/mm), (b) intermediate (1 and 30 MPa, 0 and 1.5 kV/mm), and (c) low (1 MPa and 100 V/mm) levels.

Figure 7a and 7b show the descending curves based on the estimated Ericsson cycles at intermediate level (under compressive stresses of 1 and 30 MPa) and high level (under compressive stresses of 1 and 100 MPa), respectively. The energy densities were calculated and compared to those obtained from the actual experimental Ericsson cycles, as shown in Figure 7c. For the tested samples, the energy densities obtained by the descending curves based on the estimated Ericsson cycles (Estimation 1) were inaccurate and much larger than those obtained by the actual Ericsson cycles. This difference was attributed to the hysteretic nature of the sample response. An alternative semi-empirical estimation technique based on the first-order reversal curve was proposed to address this issue. Figure 8 shows the estimated Ericsson cycles for PZT C6, C9, PMN-25PT, PZN-8PT, and PMN 15, under high variations of 1 to 100 MPa compressive stresses, using this approach.

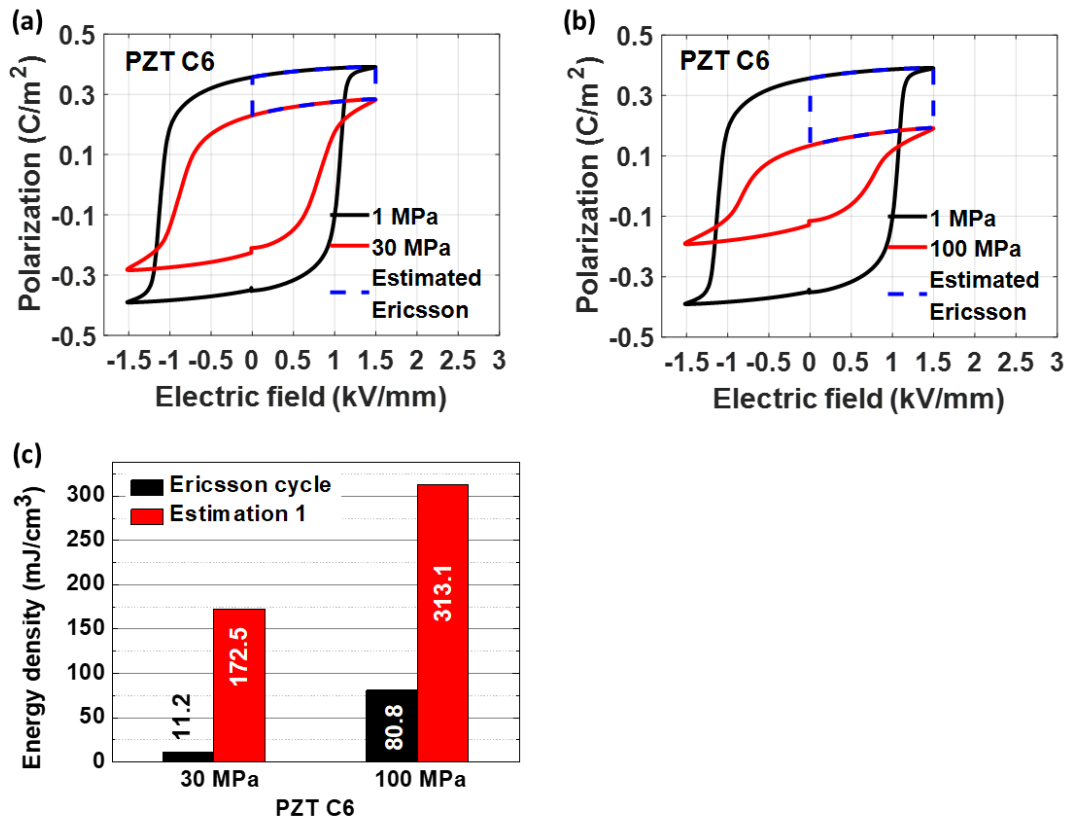


Figure 7: Descending-descending curves based on the estimated Ericsson cycles for PZT C6 under compressive stresses of (a) 1 and 30 MPa and (b) 1 and 100 MPa, and (c) comparison of energy density estimation using the actual Ericsson cycles and descending-descending curves based on the estimated Ericsson cycles (Estimation 1) of PZT C6.

The energy densities were calculated and compared to those obtained by the experimental Ericsson cycles, as shown in Figure 8f. These results indicated that the energy densities of the samples obtained using this method were much closer to those obtained by the real measured cycles for PZT C6 and C9, and slightly larger for PMN-25PT, PZN-8PT, and PMN15. Figure 9 depicts the estimated Ericsson cycles for PZT C6, C9, PMN-25PT, PZN-8PT, and PMN 15 under intermediate variations of 1 to 30 MPa of compressive stress. The energy densities were calculated and compared to those obtained from the actual experimental Ericsson cycles at an intermediate level, as shown in Figure 9f. The results indicated that the energy densities obtained by the estimated Ericsson cycles were 2 to 3 times larger than those obtained experimentally, and the estimation appeared to be accurate for the 100 MPa case, but somewhat inaccurate for the 30 MPa case. The reason for the discrepancy at 30 MPa was due to two opposite effects on the polarization change in processes 2–3 (Figure 2).

- The first effect consisted of the influence of DC losses, which caused the electric charges to continuously increase during the Ericsson cycle. Consequently, this minimized the polarization drop induced by the mechanical stress in the actual Ericsson cycle, which was not considered by the estimation.

- The second effect was the influence of increasing compressive stress, which caused a polarization drop under a high electric field. For 100 MPa, the polarization drop became much larger than the polarization variations due to DC losses. As a result, although the estimation only considered polarization hysteresis, and the estimated values were quite close to the values obtained from the real Ericsson cycles for all tested materials.

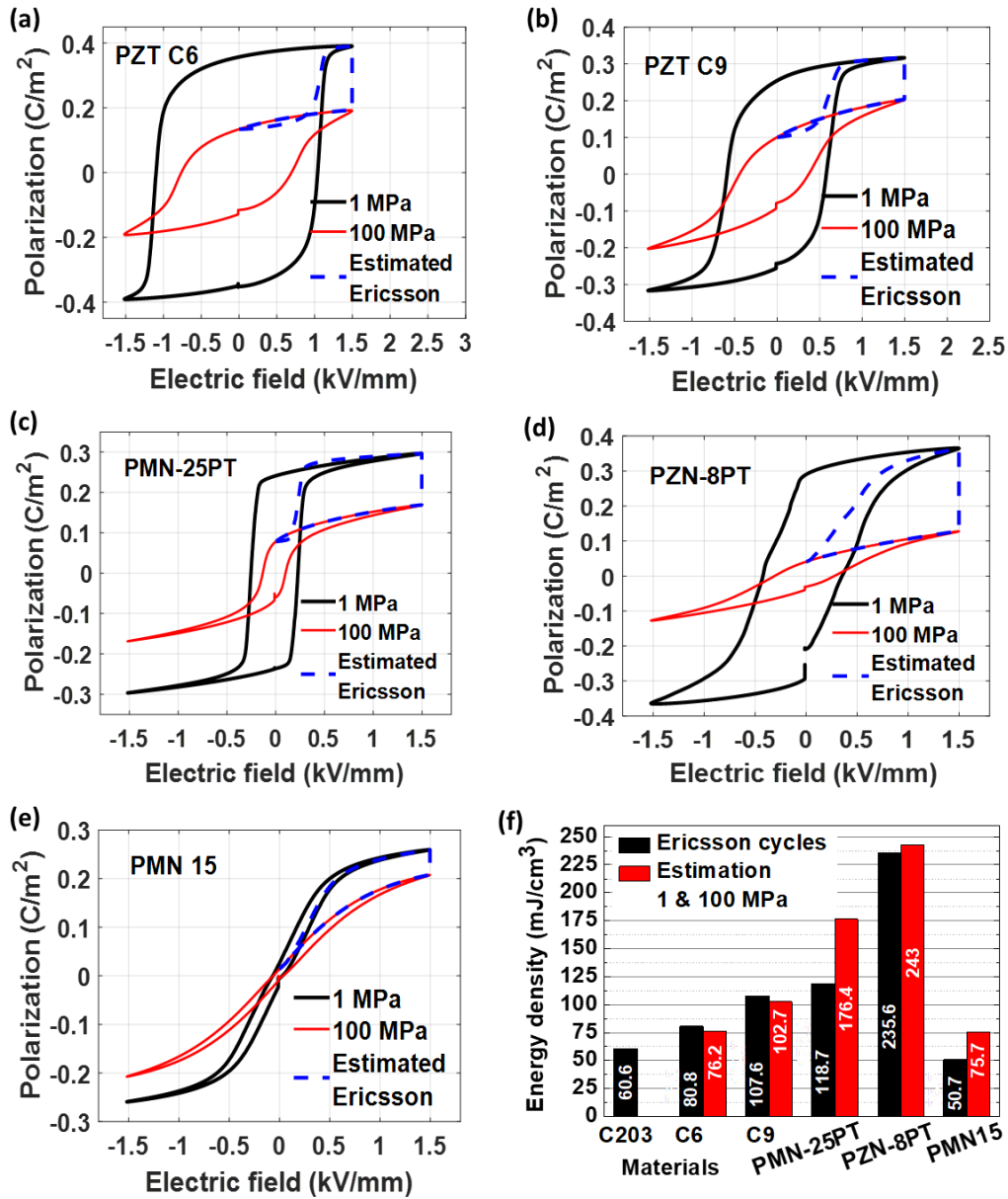


Figure 8: Proposed semi-empirical estimation technique based on the first-order reversal curve, for estimating energy densities of (a) PZT C6, (b) PZT C9, (c) PMN-25PT, (d) PZN-8PT, (e) PMN 15, and (f) combined data under compressive stress values of 1 and 100 MPa.

Of note, we expect that testing the Ericsson cycles at a much higher electric field would make both estimations similar to the actual Ericsson cycle. More precisely, if the electric field amplitude was

much larger than the coercive field, the hysteresis loss and associated irreversible polarization variation impacts would be negligible compared to the total energy density.

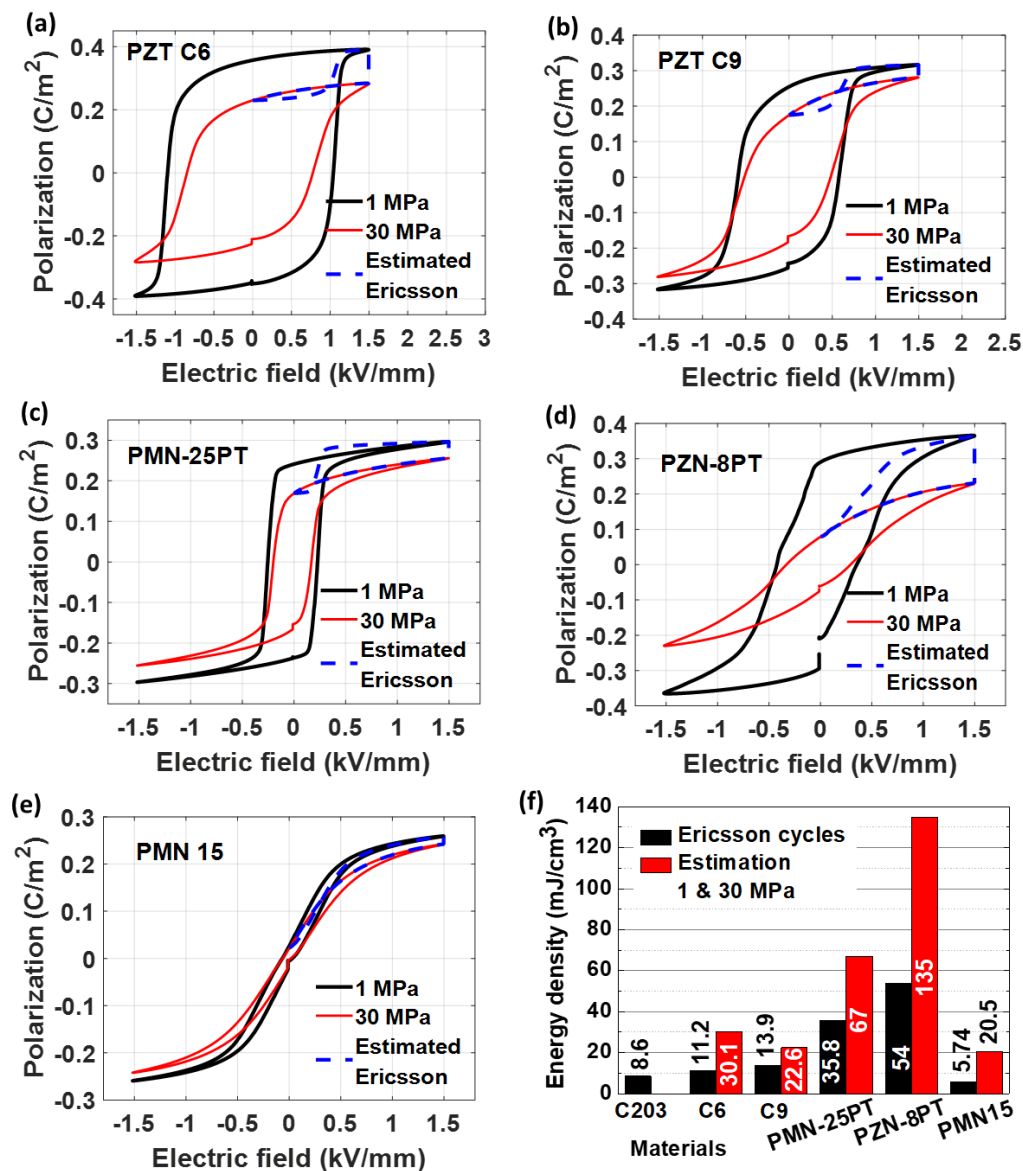


Figure 9: Estimation technique based on the first-order reversal curve for estimating the energy densities of (a) PZT C6, (b) PZT C9, (c) PMN-25PT, (d) PZN-8PT, and (e) PMN 15, and (f) combined data under compressive stress values of 1 and 30 MPa.

For PMN-25PT and PMN 15, the DC loss effect was stronger, resulting in estimated values that were slightly higher than the experimental values. At an intermediate level, the effect of DC losses was significant compared to the effect of 30 MPa of compressive stress, resulting in energy densities obtained from real Ericsson cycles that were smaller than those obtained from the estimated densities. The energy conversion performance of hard PZT C203 was not estimated under current experimental conditions (1.5 kV/mm electric field), because the bipolar hysteresis curves of hard PZT C203 were

unsymmetrical; therefore, this would require a larger electric field or higher stress, which was beyond the scope of this study.

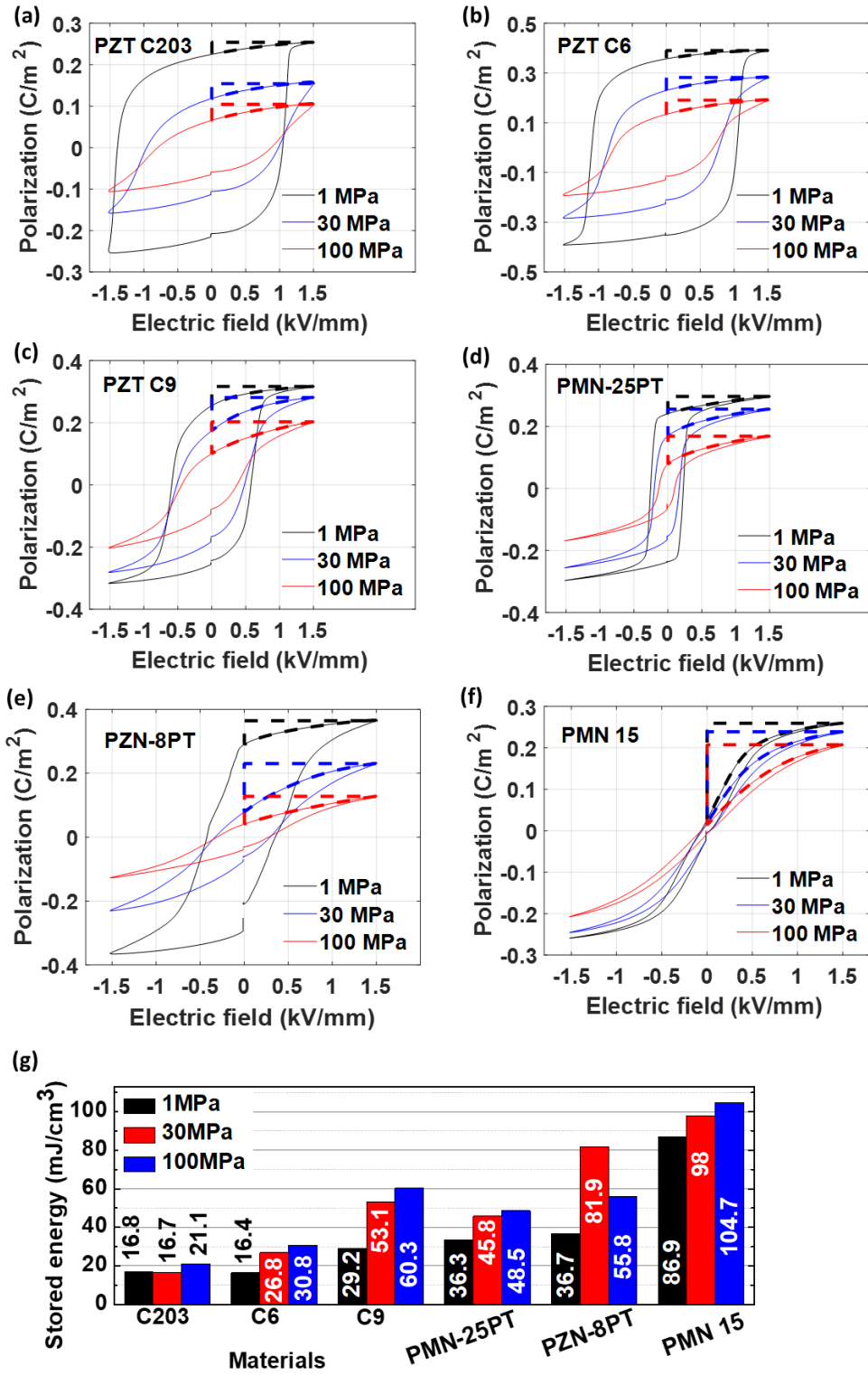


Figure 10: Energy storage capacities of PZT C203, C6, C9, PMN-25PT, PZN-8PT, and PMN 15 under compressive stress values of 1, 30, and 100 MPa.

Following this analysis, we further studied the potential applications of these ferroelectric materials in the field of electrical energy storage, and the stored energy in the samples was estimated, as shown in [Figure 10](#), while the combined data are shown in [Figure 10f](#). The results indicated that the static mechanical compressive stress could enhance the stored energy for all samples, except PZN-8PT at 30 MPa. In the case of 100 MPa, the gain in energy storage ranged from +20% to +100%, depending on the materials, and the mechanical stress tended to decrease the remnant polarization. If the saturation polarization was still of a high value, the energy density increased as it was roughly proportional to the difference between the saturation polarization and the remnant one. The highest gain was observed for PZT C9 (+100%), with its behavior under 100 MPa favoring a significant difference between remnant and saturation polarization. Unlike electromechanical energy conversion, where the paraelectric phase PMN 15 exhibited the lowest performance, the paraelectric material showed the highest level of energy storage. Because the stored energy was estimated by the surface integral of the bipolar P-E loops with polarization values from remnant to saturation polarization, the paraelectric phase PMN 15 had the smallest remnant polarization compared to the other materials; therefore, the stored energy of PMN 15 was the largest.

## 4. Discussion

### 4.1. Energy conversion ability

For applications of piezoelectric materials featuring low excitation level, such as sensors, energy harvesting, or to some extent power transducers, performance can usually be assessed by considering the materials' linear properties. For example, in resonant energy harvesting systems, the electromechanical coupling factor  $k^2$  of the system along with the mechanical quality factor  $Q_m$  of the resonator will play important roles [43,44]. However, in other analyses, the products of piezoelectric constants  $d$  and  $g$  were more relevant, depending on the mechanical excitation of the material [45]. In Ericsson cycles used for electromechanical energy conversion, with a fully controlled electric field and mechanical stress, the converted energy density, i.e., the area enclosed by points 1 to 4 in [Figure 2b](#), was only dependent on the effective  $d_{33\_eff}$  coefficient, as given in Eq. 5. Of note, the ranking of the materials followed their  $d_{33}$  values for low levels and even for intermediate levels. However, at the higher electric field and mechanical stress levels, the output energies converged due to polarization saturation, which was mainly dependent on the dipole moment and dipole density. For example, for low-level energy harvesting, the energy ratio of PZT C9 and PMN-25PT was given by the ratio of  $d_{33}$ , which was approximately 2.2 times larger for PMN-25PT. For energy cycles of 100 MPa and 1.5 kV/mm, this ratio dropped to roughly 1.1.

PZN-8PT requires additional analysis, as it did not follow this trend. This material exhibited multiple phase transitions under the conditions of mechanical stress, electric field, and temperature [46,47]. From the experimental results obtained in this study, it appeared that the effective  $d_{33\_eff}$  value remained very high, even under 1.5 kV/mm. Hence, the polarization decrease was significant due to the mechanical stress. This likely occurred because of the phase transition induced by the stress, although further investigations will be necessary to verify this assumption.

The overall convergence of all materials was further analyzed by considering the weak scattering of the spontaneous polarization among the ferroelectric materials, ranging from 0.15 to 0.4 C/m<sup>2</sup> for typical materials [48,49]. If the electric field was high enough to entirely saturate the material, and if the mechanical stress was sufficient to completely depolarize the material, then the converted energy would be similar for all tested materials. In this work, both the electric field and mechanical stress were far from these ideal conditions, resulting in a ranking between the materials by a factor of four, in terms of the converted energy from the lowest to the highest, especially in the vicinity of the phase transitions induced by both the electric field and mechanical stress.

Considering an electric field value of 1.5 kV/mm and saturation polarization of 0.4 C/m<sup>2</sup>, the ultimate energy density would be 600 mJ/cm<sup>3</sup>. The experimental results obtained in this study ranged from 50 mJ/cm<sup>3</sup> to 236 mJ/cm<sup>3</sup>, with the latter representing 40% of the ultimate energy density.

Furthermore, the output energy was dependent on the chosen electric field of the Ericsson cycle. Applying an electric field that was two times larger would approximately double the output energy. By contrast, depolarization induced by the mechanical stress would not be proportional to the stress level, and would quickly saturate when most of the polarization was already lost. Regarding the limit of the electric field, it was directly related to the dielectric strengths of the materials. In the case of bulk ferroelectric materials, applications working close to the limit can be related to power transducers and electrocaloric materials [50]. The dielectric strength can be related to the probability of finding defects in ceramics and single crystals and will be lower for bulk materials than thick and thin films. For bulk ceramics, the values range from 5 kV/mm to 15 kV/mm [51–53], while higher values have been successfully tested for single crystals [54]. In the case of thick films (typically those deposited to form multilayer capacitors), to maintain a safe level of the electric field, piezoelectric layers will usually be limited to 3 kV/mm [55], although some attempts on multi-layered capacitors have allowed tests up to 15 kV/mm [56]. Considering the previous limits, a limit value of 1.5 kV/mm could possibly be increased up to 3 to 10 times higher for some compounds, although the fatigue life might significantly decrease [57]. Regarding the mechanical stress limit, a combined application of an electric field and stress could possibly lead to premature fatigue with stress as low as 100 MPa [58]. Consequently, in this study, the electric field was limited to 1.5 kV/mm and the stress was 100 MPa. However, further detailed analysis will be necessary to explore the upper limits of the different

materials. Nonetheless, the orders of magnitude should not be significantly modified as a margin of improvement, for both limits might remain weak for bulk materials when considering high cycle capability. Furthermore, the selected limits are in line with targeted application of left-behind devices operating without any maintenance.

Interestingly, the order of magnitude in terms of energy density for all materials was in the same range as pyroelectric energy harvesting under significant temperature variations, reaching a few hundred  $\text{mJ}/\text{cm}^3/\text{cycle}$  [59]. Generally speaking, this convergence was attributed to the trade-off between the input energy (higher in thermal input and lower for mechanical excitation) and the conversion abilities (higher electromechanical coupling coefficient compared to electrothermal).

However, the use of Ericsson cycles on piezoelectric materials would not provide particular advantages in all applications of mechanical to electrical energy conversion. In the case of energy harvesting from vibration using resonant systems, provided that the electromechanical coupling  $k^2$  and mechanical quality factor  $Q_m$  were sufficiently high ( $k^2Q_m \gg 1$ ), energy harvesting would result in a strong damping effect. In such a case, the standard energy harvesting processes could convert as much energy as possible with known strategies. By contrast, in the case of weakly coupled problems, or for a non-resonant mechanical source, the best strategy would be to maximize the energy conversion per cycle. A similar situation was already encountered in the case of pyroelectric energy harvesting. Due to low electrothermal coupling, the energy conversion strategy had little impact on the input thermal energy; thus, the Ericsson cycles – also known as Olsen cycles in several works – brought much larger energy conversion density compared to the use of the solely linear pyroelectric coefficient [60][61]. Not only could Ericsson cycles be employed, but several thermodynamic cycles could also be envisaged, such as Stirling or Brayton cycles, each providing specific advantages about its feasibility and energy density [62]. Looking back to the electromechanical energy conversion, it is possible that a case study could consist of energy conversion from a single mechanical source displacement at a given force, like those encountered on roads [26][63], pathways, or sea waves [64].

#### ***4.2. Practical implementation of Ericsson cycles***

Even if we exposed and discussed the energy conversion abilities of the ferroelectric or dielectric materials, the actual implementation of the associated electrical interface was outside the scope of this study. Some preliminary considerations could still be drawn regarding the practical realization of these cycles. More precisely, practical implementation of long-term energy harvesting strategies cannot include external battery unless the scheme encompasses recharging.

In this view, a potential solution would involve circuits with a bidirectional energy flow, including controlled switches for electrically charging and discharging the active element (transducer).

According to the previously exposed constraints regarding energy self-consistency, a pre-charged battery or capacitor, with a value much larger than the maximum transducer capacitance, could also harvest energy when discharging the transducer. For example, a possible implementation would consist of DC/DC switched converters (Figure 11). Specifically, the application of an electric field in the transducer could be performed using a buck converter that was activated as the stress was applied, while the energy recovery phase (electric field release) could be achieved using a boost converter. Additionally, a diode could be placed in an anti-parallel configuration with the transducer, to prevent inverse conduction. As a first approximation, the transducer was modeled as a variable capacitor whose capacitance was related to the mechanical excitation, and Figure 12 depicts the obtained simulation implementation and results. Thus, the obtained cycles were consistent with those experimentally achieved in previous investigations. However, a storage capacitor much larger than the maximum transducer capacitance was required to maintain a constant voltage during the charging phase. Otherwise, the applied voltage would change during the process.

Furthermore, according to the energy cycle (Figure 12c), the clamped voltage increased with time. This was explained by the harvesting process, where the additional energy that was transferred to the storage stage, made of the capacitor, actually increased the voltage of the capacitor. This type of voltage increase was eventually limited by the losses within the circuit or simply by the energy consumed by the load (e.g., sensor), and this type of a voltage-constrained approach could also be implemented without an inductor, but at the cost of more complex switching topology and control [65].

However, the previously exposed scheme required active switches, for instance those composed of transistors, driven by signals that were synchronized to mechanical excitation. Although the generation of these control signals and their synchronization required minimal energy, their implementation could potentially yield some complexity that may compromise the energy balance, as the harvested energy may not be sufficient.

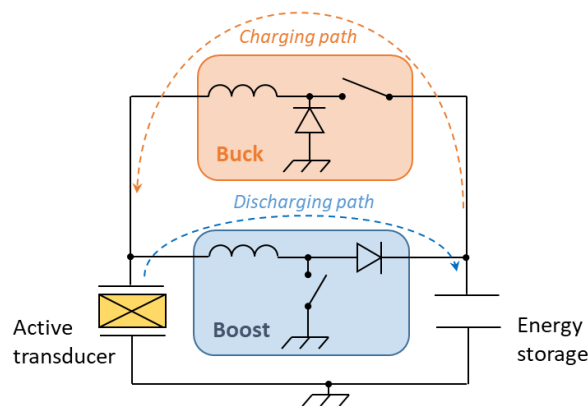


Figure 11: Implementation of the Ericsson cycle using DC/DC switched converters.

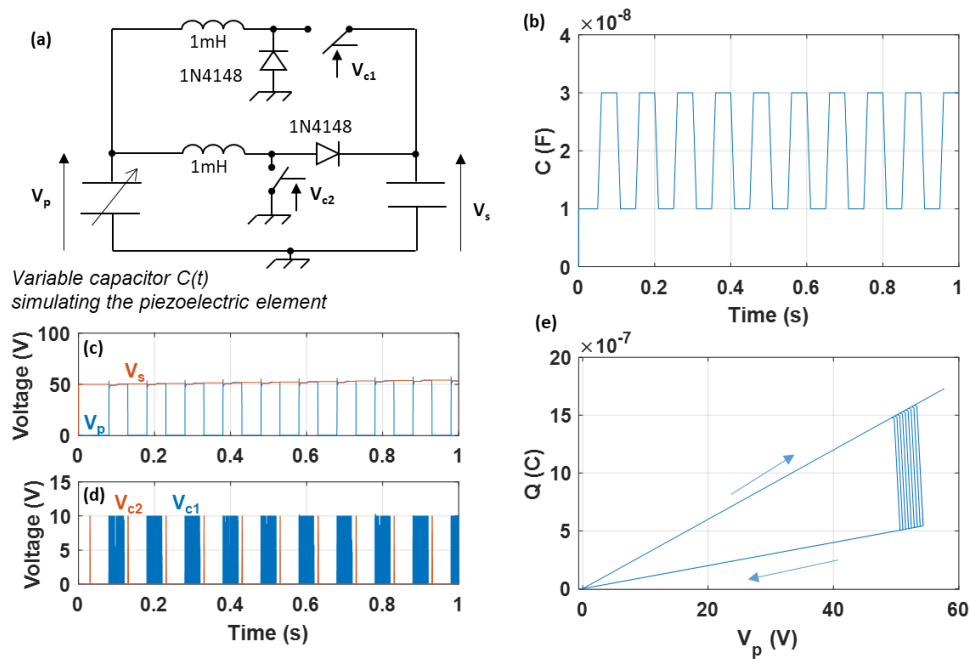


Figure 12: Simulation of the electrical interface based on the switched converters: (a) schematic, (b) time-domain waveform of the transducer capacitance  $C(t)$ , (c)  $V_p$  and  $V_s$ , the transducer and energy storage terminals, (d)  $V_{c1}$  and  $V_{c2}$ , the switch commands for charging and discharging circuits, and (e) energy cycle  $Q$  vs  $V_p$ , where  $Q$  denotes the transducer capacitance charge.

Another approach that did not directly involve Ericsson cycles consisted of self-synchronous converters as the Bennett doubler, where an overlap between mechanical excitation and electrical changes appeared [66]. This type of approach showed a significant advantage, i.e., once pre-charged, it provided a virtuous energy cycle loop in a purely passive way, without requiring any switch control; therefore, it provided significant energy savings. A simulation example is shown in Figure 13, which was still based on a variable capacitor. Hence, while not precisely an Ericsson cycle due to non-zero voltage discharge and overlap between mechanical excitation and electric field, the obtained results still shared strong similarities with the previously presented principles. Hence, we inferred that the relative material performance would be similar. Finally, we noted that such a self-synchronous structure could be enhanced by including multi-stage feedback loops that can handle limited capacitance variations [67].

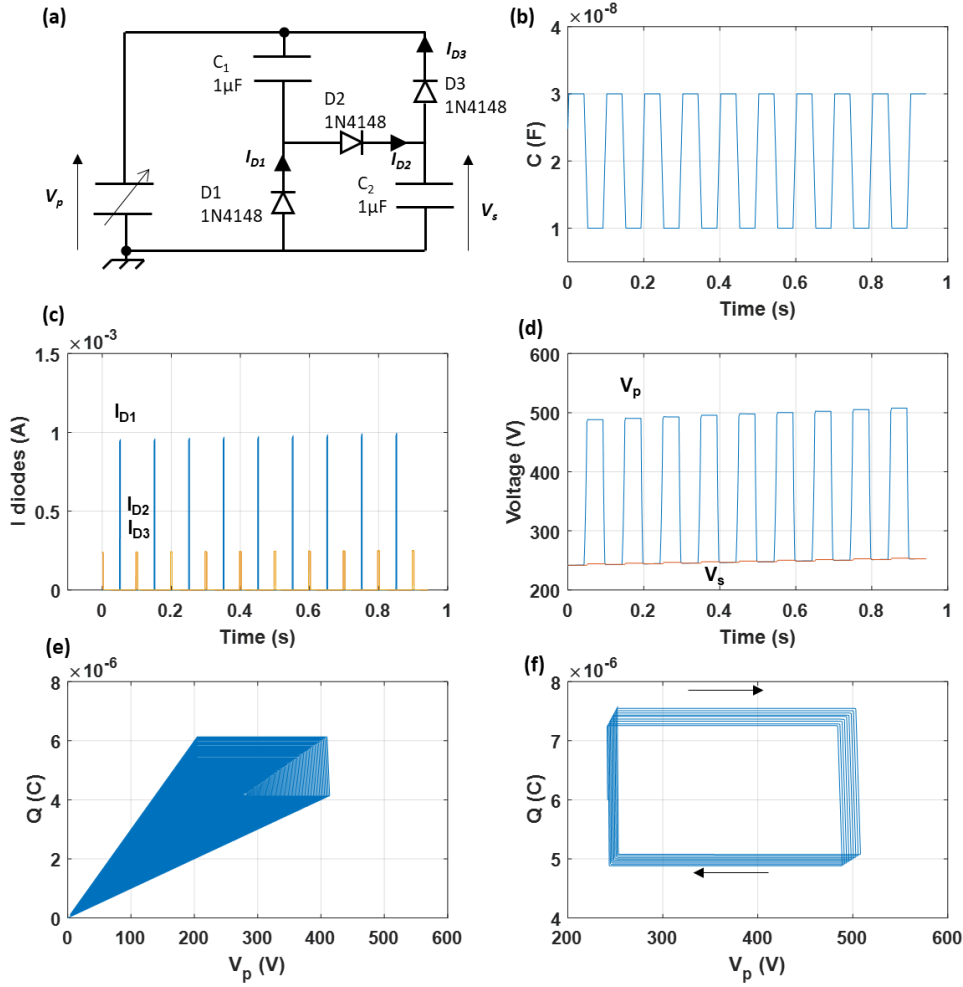


Figure 13: Simulation of the electrical interface using self-synchronous converter: (a) schematic, (b) time-domain waveform of the transducer capacitance  $C(t)$ , (c) currents in the diodes (steady-state current in diode D3 is the same as in diode D2), (d) voltages of the transducer  $V_p$  and of the storage capacitance  $V_s$ , (e) energy cycle (transient), (f) energy cycle (steady-state), where  $Q$  denotes the charge.

## 5. Conclusions

In this work, the electromechanical energy conversion performance of various ferroelectric (hard PZT C203 ceramic, medium PZT C6 ceramic, soft PZT C9 ceramic, and PMN-25PT and PZN-8PT single crystal) and paraelectric (PMN 15 ceramic) materials was investigated using Ericsson cycles under intermediate and high compressive stress levels (30 MPa and 100 MPa) with an electric field of 1.5 kV/mm and at room temperature (20°C). The ferroelectric PZN-8PT single crystal exhibited the highest potential for energy conversion among the assessed materials, with an energy density reaching 235.6 mJ/cm<sup>3</sup>. However, under high electric field and stress levels, the energy conversion performance of the PZT C9 ceramic was found to be comparable to the PMN-25PT single crystal, with an energy

density of 118.7 mJ/cm<sup>3</sup>. PZT C9 was found to be an excellent candidate for practical applications due to its well-established commercial fabrication routes, yielding an affordable transducer. Measurement of the Ericsson cycle remained a time-consuming process, as it required complete control of the electric field and stress with time, along with their synchronization. Thus, a simple and accurate semi-empirical estimation technique was proposed to evaluate the energy conversion performance of the ferroelectric materials via the compressive stress-induced bipolar hysteresis curves. This was found to be much more precise, compared to solely relying on the descending hysteresis P-E curves. Estimations using this approach were accurate for PZT C6, C9, and PZN-8PT and slightly larger for PMN 15 and PMN-25PT compared to the experimental results. The acquisition of bipolar hysteresis curves was easier than the Ericsson cycles; thus, this method permitted the fast screening of ferroelectric materials. The results obtained in this study were dependent on the electric field amplitude used during the Ericsson cycle measurements. Consequently, a higher dielectric strength for a given material might allow for a larger electric field and output energy. Nevertheless, utilizing a safe operating condition (which is necessary for ensuring reliable operation of the device in the long term) in the kV/mm range for bulk ferroelectrics led to energy in the hundreds of mJ/cm<sup>3</sup>. Increasing the electric field amplitude by a factor of 10 (highest dielectric strength on bulk ferroelectrics) would lead to an energy density in the J/cm<sup>3</sup> range at the highest.

Lastly, we further studied the potentials of these materials for electrical energy storage applications. The maximum obtained stored energy was found to be 104.7 mJ/cm<sup>3</sup> for the paraelectric PMN 15 ceramic at a high level of 100 MPa compressive stress. In contrast to electromechanical energy conversion, in which paraelectric PMN 15 exhibited the lowest performance compared to the other ferroelectric materials, in terms of energy storage, PMN 15 had the highest amount of stored energy. This study paves the way for future applications of these materials for energy harvesting and energy storage.

### **Acknowledgments**

This work was performed under the framework of the ANR-FIESTA project, funded by the French Agence Nationale pour la Recherche, grant #ANR-20-CE05-0026, and under the framework of the International Research Network ELyT Global.

### **Data availability**

The data that support the findings of this study are available from the corresponding authors upon reasonable request

## Corresponding authors

Correspondence to Gael Sebald & Nguyen Thanh Tung

## Contributions

Gael Sebald, Mickaël Lallart and Elie Lefevre conceived and designed the research; Nguyen Thanh Tung and Gael Sebald performed the experiment and analyzed the data; Nguyen Thanh Tung, Gael Sebald, Mickaël Lallart, Elie Lefevre, and Benjamin Ducharne wrote the manuscript; other authors contributed to research discussion; all authors reviewed and edited the manuscript; Mickaël Lallart and Gaël Sebald secured funding.

## Conflict of interests

The authors declare that they have no competing interests.

## References

1. Bowen CR, Kim HA, Weaver PM, Dunn S. 2014 Piezoelectric and ferroelectric materials and structures for energy harvesting applications. *Energy Environ. Sci.* **7**, 25–44. (doi:10.1039/C3EE42454E)
2. Mane P, Xie J, Leang KK, Mossi K. 2011 Cyclic energy harvesting from pyroelectric materials. *IEEE Trans. Ultrason. Ferroelectr. Freq. Control* **58**, 10–17. (doi:10.1109/TUFFC.2011.1769)
3. Wu L, Wang X, Li L. 2016 Lead-free BaTiO<sub>3</sub>–Bi(Zn<sup>2/3</sup>Nb<sup>1/3</sup>)O<sub>3</sub> weakly coupled relaxor ferroelectric materials for energy storage. *RSC Adv.* **6**, 14273–14282. (doi:10.1039/C5RA21261H)
4. Zhao P, Wang H, Wu L, Chen L, Cai Z, Li L, Wang X. 2019 High-Performance Relaxor Ferroelectric Materials for Energy Storage Applications. *Adv. Energy Mater.* **9**, 1803048. (doi:10.1002/aenm.201803048)
5. Kumar A, Kim SH, Peddigari M, Jeong D-H, Hwang G-T, Ryu J. 2019 High Energy Storage Properties and Electrical Field Stability of Energy Efficiency of (Pb<sub>0.89</sub>La<sub>0.11</sub>)(Zr<sub>0.70</sub>Ti<sub>0.30</sub>)<sub>0.9725</sub>O<sub>3</sub> Relaxor Ferroelectric Ceramics. *Electron. Mater. Lett.* **15**, 323–330. (doi:10.1007/s13391-019-00124-z)
6. Guo R, You L, Zhou Y, Shih Lim Z, Zou X, Chen L, Ramesh R, Wang J. 2013 Non-volatile memory based on the ferroelectric photovoltaic effect. *Nat. Commun.* **4**, 1990. (doi:10.1038/ncomms2990)
7. Garcia V, Bibes M. 2014 Ferroelectric tunnel junctions for information storage and processing. *Nat. Commun.* **5**, 4289. (doi:10.1038/ncomms5289)

8. Papagiannakis AT, Dessouky S, Montoya A, Roshani H. 2016 Energy Harvesting from Roadways. *Procedia Comput. Sci.* **83**, 758–765. (doi:10.1016/j.procs.2016.04.164)
9. Wu M, Yao K, Li D, Huang X, Liu Y, Wang L, Song E, Yu J, Yu X. 2021 Self-powered skin electronics for energy harvesting and healthcare monitoring. *Mater. Today Energy* **21**, 100786. (doi:10.1016/j.mtener.2021.100786)
10. Zhao Z, Dai Y, Dou SX, Liang J. 2021 Flexible nanogenerators for wearable electronic applications based on piezoelectric materials. *Mater. Today Energy* **20**, 100690. (doi:10.1016/j.mtener.2021.100690)
11. Prauzek M, Konecny J, Borova M, Janosova K, Hlavica J, Musilek P. 2018 Energy Harvesting Sources, Storage Devices and System Topologies for Environmental Wireless Sensor Networks: A Review. *Sensors* **18**, 2446. (doi:10.3390/s18082446)
12. Kim TY, Kim SK, Kim S-W. 2018 Application of ferroelectric materials for improving output power of energy harvesters. *Nano Converg.* **5**, 30. (doi:10.1186/s40580-018-0163-0)
13. Liu M, Mi J, Tai W-C, Zuo L. 2021 A novel configuration for high power-output and highly efficient vibration energy harvesting. *Appl. Energy* **295**, 116957. (doi:10.1016/j.apenergy.2021.116957)
14. Na Y, Lee M-S, Lee JW, Jeong YH. 2020 Wind energy harvesting from a magnetically coupled piezoelectric bimorph cantilever array based on a dynamic magneto-piezo-elastic structure. *Appl. Energy* **264**, 114710. (doi:10.1016/j.apenergy.2020.114710)
15. Vocca H, Neri I, Travasso F, Gammaitoni L. 2012 Kinetic energy harvesting with bistable oscillators. *Appl. Energy* **97**, 771–776. (doi:10.1016/j.apenergy.2011.12.087)
16. Romero E, Warrington RO, Neuman MR. 2009 Energy scavenging sources for biomedical sensors. *Physiol. Meas.* **30**, R35–R62. (doi:10.1088/0967-3334/30/9/R01)
17. Defosseux M, Allain M, Ivaldi P, Defay E, Basrour S. 2011 Highly efficient piezoelectric micro harvester for low level of acceleration fabricated with a CMOS compatible process. In *2011 16th International Solid-State Sensors, Actuators and Microsystems Conference*, pp. 1859–1862. IEEE. (doi:10.1109/TRANSDUCERS.2011.5969866)
18. Elfrink R, Kamel TM, Goedbloed M, Matova S, Hohlfeld D, van Andel Y, van Schaijk R. 2009 Vibration energy harvesting with aluminum nitride-based piezoelectric devices. *J. Micromechanics Microengineering* **19**, 094005. (doi:10.1088/0960-1317/19/9/094005)
19. Starner T. 1996 Human-powered wearable computing. *IBM Syst. J.* **35**, 618–629. (doi:10.1147/sj.353.0618)
20. Vats G, Singh Kushwaha H, Vaish R. 2014 Enormous energy harvesting and storage potential in multiferroic epitaxial thin film heterostructures: an unforeseen era. *Mater. Res. Express* **1**, 015503. (doi:10.1088/2053-1591/1/1/015503)
21. Sebald G, Pruvost S, Guyomar D. 2008 Energy harvesting based on Ericsson pyroelectric cycles in a relaxor ferroelectric ceramic. *Smart Mater. Struct.* **17**, 015012. (doi:10.1088/0964-1726/17/01/015012)

22. Unruan M, Unruan S, Inkong Y, Yimmirun R. 2019 Estimation of energy density of PMN-PT ceramics utilizing mechanical stress. *Integr. Ferroelectr.* **195**, 39–45. (doi:10.1080/10584587.2019.1570042)
23. Patel S, Chauhan A, Vaish R. 2014 Enhanced energy harvesting in commercial ferroelectric materials. *Mater. Res. Express* **1**, 025504. (doi:10.1088/2053-1591/1/2/025504)
24. Bakshi AN, Moghal AAB, Madhar NA, Patel S, Vaish R. 2015 Effect of Stress on Energy Conversion and Storage Characteristics of (1-x-y)PIN-xPMN-yPT Single Crystals. *Ferroelectr. Lett. Sect.* **42**, 107–114. (doi:10.1080/07315171.2015.1068507)
25. Smith AN, Hanrahan BM. 2020 Cascaded pyroelectric conversion: Optimizing the ferroelectric phase transition and electrical losses. *J. Appl. Phys.* **128**, 024103. (doi:10.1063/5.0003301)
26. Chen C, Xu T-B, Yazdani A, Sun J-Q. 2021 A high density piezoelectric energy harvesting device from highway traffic — System design and road test. *Appl. Energy* **299**, 117331. (doi:10.1016/j.apenergy.2021.117331)
27. Zhang B, Duchame B, Sebald G, Guyomar D. 2014 Energy harvesting based on piezoelectric ericsson cycles in a piezoceramic material. In *2014 Joint IEEE International Symposium on the Applications of Ferroelectric, International Workshop on Acoustic Transduction Materials and Devices & Workshop on Piezoresponse Force Microscopy*, pp. 1–4. IEEE. (doi:10.1109/ISAF.2014.6923021)
28. Zhang B, Ducharne B, Guyomar D, Sebald G. 2013 Energy harvesting based on piezoelectric Ericsson cycles in a piezoceramic material. *Eur. Phys. J. Spec. Top.* **222**, 1733–1743. (doi:10.1140/epjst/e2013-01958-0)
29. Kounga AB, Granzow T, Aulbach E, Hinterstein M, Rödel J. 2008 High-temperature poling of ferroelectrics. *J. Appl. Phys.* **104**, 024116. (doi:10.1063/1.2959830)
30. Matsushima M, Tachi Y, Iwasaki Y. 2005 Development of large diameter piezo-single crystal PMN-PT with high energy conversion efficiency. *JFE Tech. Rep.* , 46–51.
31. Poterala SF, Trolrier-McKinstry S, Meyer RJ, Messing GL. 2011 Processing, texture quality, and piezoelectric properties of <001> C textured (1-x)Pb(Mg 1/3 Nb 2/3 )TiO 3 - xPbTiO 3 ceramics. *J. Appl. Phys.* **110**, 014105. (doi:10.1063/1.3603045)
32. Ren W, Masys AJ, Yang G, Mukherjee BK. 2002 Nonlinear strain and DC bias induced piezoelectric behaviour of electrostrictive lead magnesium niobate-lead titanate ceramics under high electric fields. *J. Phys. D. Appl. Phys.* **35**, 316. (doi:10.1088/0022-3727/35/13/316)
33. Pan M-J, Rehrig PW, Kucera JP, Park SEE, Hackenberger WS. 2000 Comparison of actuator properties for piezoelectric and electrostrictive materials. In (ed CS Lynch), pp. 80–90.(doi:10.1117/12.388248)
34. JI DW, KIM S-J. 2016 Compressive stress-induced depolarization in ferroelectric ceramics at room and high temperatures: experiment and prediction. *J. Ceram. Soc. Japan* **124**, 1132–1140. (doi:10.2109/jcersj2.16135)
35. JI DW, KIM S-J. 2018 Nonlinear behavior of ferroelectric ceramics during mechanical

- depolarization at room and high temperatures: experiment and prediction by an experimental formula. *J. Ceram. Soc. Japan* **126**, 39–49. (doi:10.2109/jcersj2.17084)
36. Yimnirun R, Triamnak N, Unruan M, Ngamjarrojana A, Laosiritaworn Y, Ananta S. 2009 Stress-dependent ferroelectric properties of  $\text{Pb}(\text{Zr}_{1/2}\text{Ti}_{1/2})\text{O}_3$ – $\text{Pb}(\text{Zn}_{1/3}\text{Nb}_{2/3})\text{O}_3$  ceramic systems. *Ceram. Int.* **35**, 185–189. (doi:10.1016/j.ceramint.2007.10.036)
  37. Unruan M, Ananta S, Laosiritaworn Y, Ngamjarrojana A, Guo R, Bhalla A, Yimnirun R. 2010 Effects of Parallel and Perpendicular Compressive Stresses on the Dielectric and Ferroelectric Properties of Soft PZT Ceramics. *Ferroelectrics* **400**, 144–154. (doi:10.1080/00150193.2010.505517)
  38. Nguyen H, Navid A, Pilon L. 2010 Pyroelectric energy converter using co-polymer P(VDF-TrFE) and Olsen cycle for waste heat energy harvesting. *Appl. Therm. Eng.* **30**, 2127–2137. (doi:10.1016/j.applthermaleng.2010.05.022)
  39. Siao A-S, McKinley IM, Chao C-K, Hsiao C-C, Pilon L. 2018 Pyroelectric waste heat energy harvesting using the Olsen cycle on  $\text{Pb}(\text{Zr}, \text{Ti})\text{O}_3$ – $\text{Pb}(\text{Ni}, \text{Nb})\text{O}_3$  ceramics. *J. Appl. Phys.* **124**, 174104. (doi:10.1063/1.5037112)
  40. Goh Y, Jeon S. 2018 First-order reversal curve diagrams for characterizing ferroelectricity of  $\text{Hf}_{0.5}\text{Zr}_{0.5}\text{O}_2$  films grown at different rates. *J. Vac. Sci. Technol. B* **36**, 052204. (doi:10.1116/1.5046762)
  41. Chauhan A, Patel S, Vaish R. 2014 Mechanical confinement for improved energy storage density in BNT-BT-KNN lead-free ceramic capacitors. *AIP Adv.* **4**, 087106. (doi:10.1063/1.4892608)
  42. Patel S, Chauhan A, Vaish R. 2014 Enhancing electrical energy storage density in anti-ferroelectric ceramics using ferroelastic domain switching. *Mater. Res. Express* **1**, 045502. (doi:10.1088/2053-1591/1/4/045502)
  43. Lefevre E, Sebald G, Guyomar D, Lallart M, Richard C. 2009 Materials, structures and power interfaces for efficient piezoelectric energy harvesting. *J. Electroceramics* **22**, 171–179. (doi:10.1007/s10832-007-9361-6)
  44. Guyomar D, Richard C, Badel A, Lefevre E, Lallart M. In press. Energy Harvesting using Non-linear Techniques. In *Energy Harvesting Technologies*, pp. 209–266. Boston, MA: Springer US. (doi:10.1007/978-0-387-76464-1\_8)
  45. Deutz DB, Pascoe J-A, Schelen B, van der Zwaag S, de Leeuw DM, Groen P. 2018 Analysis and experimental validation of the figure of merit for piezoelectric energy harvesters. *Mater. Horizons* **5**, 444–453. (doi:10.1039/C8MH00097B)
  46. Davis M, Damjanovic D, Setter N. 2006 Electric-field-, temperature-, and stress-induced phase transitions in relaxor ferroelectric single crystals. *Phys. Rev. B* **73**, 014115. (doi:10.1103/PhysRevB.73.014115)
  47. Janolin P-E, Dkhil B, Davis M, Damjanovic D, Setter N. 2007 Uniaxial-stress induced phase transitions in [001]C-poled  $0.955\text{Pb}(\text{Zn}_{1/3}\text{Nb}_{2/3})\text{O}_3$ – $0.045\text{PbTiO}_3$ . *Appl. Phys. Lett.* **90**, 152907. (doi:10.1063/1.2721856)

48. Damjanovic D. 1998 Ferroelectric, dielectric and piezoelectric properties of ferroelectric thin films and ceramics. *Reports Prog. Phys.* **61**, 1267–1324. (doi:10.1088/0034-4885/61/9/002)
49. Wongdamnern N, Triamnak N, Ngamjarurojana A, Laosiritaworn Y, Ananta S, Yimnirun R. 2008 Comparative studies of dynamic hysteresis responses in hard and soft PZT ceramics. *Ceram. Int.* **34**, 731–734. (doi:10.1016/j.ceramint.2007.09.048)
50. Valant M, Axelsson A-K, Le Goupil F, Alford NM. 2012 Electrocaloric temperature change constrained by the dielectric strength. *Mater. Chem. Phys.* **136**, 277–280. (doi:10.1016/j.matchemphys.2012.08.059)
51. Takeda S, Uchimoto T, Kita A, Matsumoto T, Sasaki T. 2021 Mechanism study of the residual stress evaluation of low-carbon steels using the eddy current magnetic signature method. *J. Magn. Mater.* **538**, 168268. (doi:10.1016/j.jmmm.2021.168268)
52. Gerson R, Marshall TC. 1959 Dielectric Breakdown of Porous Ceramics. *J. Appl. Phys.* **30**, 1650–1653. (doi:10.1063/1.1735030)
53. Yang H, Dong X, Zhong N, Wang Y. 2004 Dielectric Breakdown Properties of Zr-Rich Lead Zirconate Titanate Ceramics. *Jpn. J. Appl. Phys.* **43**, 7579–7582. (doi:10.1143/JJAP.43.7579)
54. Park S-E, Shrout TR. 1997 Ultrahigh strain and piezoelectric behavior in relaxor based ferroelectric single crystals. *J. Appl. Phys.* **82**, 1804–1811. (doi:10.1063/1.365983)
55. Esteves G, Fancher CM, Röhrig S, Maier GA, Jones JL, Deluca M. 2017 Electric-field-induced structural changes in multilayer piezoelectric actuators during electrical and mechanical loading. *Acta Mater.* **132**, 96–105. (doi:10.1016/j.actamat.2017.04.014)
56. Nair B, Usui T, Crossley S, Kurdi S, Guzmán-Verri GG, Moya X, Hirose S, Mathur ND. 2019 Large electrocaloric effects in oxide multilayer capacitors over a wide temperature range. *Nature* **575**, 468–472. (doi:10.1038/s41586-019-1634-0)
57. He Z, Loh HT, Ong EH. 2005 A Probabilistic Approach to Evaluate the Reliability of Piezoelectric Micro-Actuators. *IEEE Trans. Reliab.* **54**, 83–91. (doi:10.1109/TR.2004.842089)
58. Makino H, Kamiya N. 1994 Effects of dc Electric Field on Mechanical Properties of Piezoelectric Ceramics. *Jpn. J. Appl. Phys.* **33**, 5323–5327. (doi:10.1143/JJAP.33.5323)
59. Bowen CR, Taylor J, LeBoulbar E, Zabek D, Chauhan A, Vaish R. 2014 Pyroelectric materials and devices for energy harvesting applications. *Energy Environ. Sci.* **7**, 3836–3856. (doi:10.1039/C4EE01759E)
60. Olsen RB, Bruno DA, Briscoe JM. 1985 Pyroelectric conversion cycles. *J. Appl. Phys.* **58**, 4709. (doi:10.1063/1.336244)
61. Khodayari A, Pruvost S, Sebald G, Guyomar D, Mohammadi S. 2009 Nonlinear pyroelectric energy harvesting from relaxor single crystals. *IEEE Trans. Ultrason. Ferroelectr. Freq. Control* **56**, 693–9. (doi:10.1109/TUFFC.2009.1092)
62. Pandya S, Velarde G, Zhang L, Wilbur JD, Smith A, Hanrahan B, Dames C, Martin LW. 2019 New approach to waste-heat energy harvesting: pyroelectric energy conversion. *NPG Asia Mater.* **11**, 26. (doi:10.1038/s41427-019-0125-y)

63. Yang H, Wang L, Zhou B, Wei Y, Zhao Q. 2018 A preliminary study on the highway piezoelectric power supply system. *Int. J. Pavement Res. Technol.* **11**, 168–175. (doi:10.1016/j.ijprt.2017.08.006)
64. Zhang B, Ducharne B, Gupta B, Sebald G, Guyomar D, Gao J. 2018 Experimental sea wave energy extractor based on piezoelectric Ericsson cycles. *J. Intell. Mater. Syst. Struct.* **29**, 1102–1112. (doi:10.1177/1045389X17730917)
65. Torres EO, Rincon-Mora GA. 2010 A 0.7- $\mu\text{m}$  BiCMOS Electrostatic Energy-Harvesting System IC. *IEEE J. Solid-State Circuits* **45**, 483–496. (doi:10.1109/JSSC.2009.2038431)
66. Ghaffarinejad A, Lu Y, Hinchet R, Galayko D, Hasani JY, Kim SW, Basset P. 2018 Bennet's doubler working as a power booster for triboelectric nano-generators. *Electron. Lett.* **54**, 378–379. (doi:10.1049/el.2017.3434)
67. Lefeuvre E, Risquez S, Wei J, Woytasik M, Parrain F. 2014 Self-Biased Inductor-less Interface Circuit for Electret-Free Electrostatic Energy Harvesters. *J. Phys. Conf. Ser.* **557**, 012052. (doi:10.1088/1742-6596/557/1/012052)